Molecular dynamics and crystallization in polymers based on ethylene glycol methacrylates (EGMAs) with melt memory characteristics: from linear oligomers to comb-like polymers†

Olga Vassiliadou, [ID] [a] Varvara Chrysostomou, [ID] [b] Stergios Pispas, [ID] [b] Panagiotis A. Klonos [ID] [a] and Apostolos Kyritsis [ID] *[a]

In this article we present results on the glass transition, crystallization and molecular dynamics in relatively novel oligomers, oligo-ethylene glycol methacrylate (OEGMA), with short and long chains, as well as in the corresponding nanostructured comb-like polymers (POEGMA, short and long), the latter being prepared *via* the RAFT polymerization process. For the investigation we employed conventional and temperature modulated differential scanning calorimetry in combination with high resolving power dielectric spectroscopy techniques, broadband dielectric relaxation spectroscopy (BDS) and thermally stimulated depolarization currents (TSDC). Under ambient conditions short OEGMA (475 g mol^{-1}, $\sim$4 nm in length) exhibits a remarkable low glass transition temperature, T_g, of -91 °C, crystallization temperature $T_c = -24$ °C and a significant crystalline fraction, CF, of $\sim$30%. When doubling the number of monomers (OEGMA-long, 950 g mol^{-1}, chain length $\sim$8 nm) the T_g increases by about 20 K and CF increases to $\sim$53%, whereas, the T_c migrates to a room-like temperature of 19 °C. Upon formation of comb-like POEGMA structures the grafted OEGMA short chains, strikingly, are not able to crystallize, while in POEGMA-long the crystallization behaviour changes significantly as compared to OEGMA. Our results indicate that in the comb-like architecture the chain diffusion of the amorphous fractions is also strongly affected. The semicrystalline systems exhibit significant melt memory effects, this being stronger in the comb-like architecture. It is shown that these effects are related to the inter- and intra-chain interactions of the crystallizable chains. The dielectric techniques allowed the molecular dynamics mapping of these new systems from the linear oligomers to POEGMAs for the first time. BDS and TSDC detected various dynamics processes, in particular, the local polymer dynamics (γ process) to be sensitive to the T_g, local dynamics triggered in the hydrophilic chain segments by water traces (β), as well as the segmental dynamics (α) related to glass transition. Interestingly, both the short and long linear OEGMAs exhibit an additional relaxation process that resembles the Normal-Mode process appearing in polyethers. In the corresponding POEGMAs this process could not be resolved, this being an effect of the one-side grafted chain on the comb backbone. The revealed variations in molecular mobility and crystallization behavior suggest the potentially manipulable diffusion of small molecules throughout the polymer volume, *via* both the molecular architecture as well as the thermal treatment. This ability is extremely useful for these novel materials, envisaging their future applications in biomedicine (drug encapsulation).

1. Introduction

Poly(oligo ethylene glycol methacrylate) (POEGMA), the material of interest here, belongs to a class of polymers demonstrating 'graft-like' structures composed of carbon–carbon backbones (hydrophobic) and multiple oligo(ethylene glycol) side-chains (branches)[1–3] which are hydrophilic. Such materials are usually addressed as brush- or comb-like polymers[4–8] being the non-linear poly(ethylene glycol) (PEG) analogues.[2] For short side chains, which occur for less than $\sim$10 ethylene glycol units, the POEGMA homopolymers are considered thermoresponsive, as upon thermally induced dehydration they undergo a nano-phase transition.[2,9] This transition is due to the distinct chemical nature between the backbone and the branches so that, in the presence of solvents, selective chain associations are favored

[a] Department of Physics, National Technical University of Athens, Zografou Campus, 15780, Athens, Greece. E-mail: akyrits@central.ntua.gr

[b] Theoretical and Physical Chemistry Institute, National Hellenic Research Foundation, 48 Vassileos Constantinou Avenue, 11635 Athens, Greece

† Electronic supplementary information (ESI) available. See DOI: 10.1039/d0sm01666g

(nano-domain formation).[10–13] The nano-phase transition occurs, however, without POEGMA exhibiting formation of inter- and/or intra-chain hydrogen bonds between the side chains (branches, ethylene glycol-like). Nevertheless, for longer side chains, POEGMA homopolymers lose their thermoresponsive character due to the domination of side chain associations and the formation of crystalline domains above a critical length of PEG side chains. The specific features of PEG side chain crystallization in the morphology of brush copolymers has gained significant attention during the last few years,[6,14] indicating the continued interest in the morphological behavior of this rather unique polymer.

Brush copolymers consisting of an amorphous main chain and crystallizable side chains can phase separate into a variety of morphologies resulting in copolymers with interesting properties.[5,8,15–17] The crystallization behavior of such brush polymers has been investigated in the past decades by various groups, and according to the generally most accepted model the main chain and a fraction of side chains in the vicinity of the main chain constitute the amorphous phase whereas the side chains are incorporated into crystalline lamella separated by amorphous domains.[5,16] It is widely accepted that factors such as the backbone rigidity, the nature of the linking groups, and the length of the side chains affect significantly the side chain crystallization.[5,18] In the case of PEG side chains, the reported results have indicated that the crystallization temperature, T_c, decreases as compared to linear long PEG [poly(ethylene oxide), PEO] macromolecular chains and the degree of supercooling depends strongly on the length of the side chains, with T_c ranging from slightly below 0 °C to about 65 °C.[6,14–16] Furthermore, it has been shown that crystallization in the brush copolymers was hindered by frustration in packing of the crystallizable PEG chains which can be realized either in the interdigitating or the end-to-end form.[5,15]

PEO has been widely employed as a crystallizable block copolymer component, in various polymer architectures like, for example, block-copolymers and star-like structures, leading to a great diversity of literature reports on its crystallization temperature as a function of morphology,[6] usually far below the PEO equilibrium melting temperature, T_m, of 76 °C.[19] The dynamic crystallization of homogeneously nucleated PEO nanodroplets has been reported in the range between −30 and −45 °C (peak crystallization temperatures during cooling from the melt), *i.e.* quite close to the glass transition temperature, T_g, for small PEO microdomains.[20] Interestingly, when confining bulk PEO in self-ordered nanoporous anodic aluminum oxide (AAO) with a pore diameter of 25 nm, the homogeneous nucleation crystallization temperature has been observed to be as low as −38.8 °C.[21] Strong PEO supercooling effects have usually been interpreted as manifestations of the homogeneous nucleation process for PEO chains. For PEO homopolymers, similarly to other macromolecules, the heterogeneous nucleation process has been suggested as the main crystallization mechanism.[22] However, it has been demonstrated that 'melt memory effects' lead to a special case of homogeneous nucleation for PEO homopolymers as well as other macromolecules.[2] The melt memory is a common phenomenon

in polymer crystallization where recrystallization of a semicrystalline polymer depends strongly on the existence of the so-called "*melt structure*" of its previous molten state.[22–25] Depending on the temperature of the melt and/or the annealing time in the molten state, the molten state may retain a "*melt structure*" with preserved orientation of the chains. This orientation originates initially from the chain conformations in the crystalline structures or is produced by sticky chain associations of the chains in the melt, due to inter-chain segmental contacts, for example *via* formation of inter/intramolecular hydrogen bonds or other types of weak forces.[22,26,27] During re-crystallization of the macromolecular chains, an increase in T_c (and the crystallization rate) is observed, caused by a self-nucleation process, and the effect is known as the melt memory effect. The strength and specific features of the melt memory effect may offer an additional tool for assessing the degree of complexity in the macromolecular structure and dynamics of various chain architectures due to the existing chain associations and structural constraints.

In the present work we investigate, for the first time, the crystallization behavior, thermal transitions and molecular dynamics of POEGMA homopolymers with PEG side chains of two different and rather short lengths. Such materials aim at drug delivery applications, therefore the deeper scope here is the extraction of information on the ability to tune the crystallinity parameters as well as the diffusion of small molecules (ions, water, drug solutions) *via* these materials. In order to study the chain architecture effects, *i.e.* that the crystallizable chain is anchored to the polymer backbone, the corresponding free oligomeric chains (OEGMA) will be studied in parallel. The results of this study will be discussed also in the light of recent findings in similar oligomers.[28,29] Among the most effective tools for studying molecular dynamics in polymers are the dielectric spectroscopy techniques[30–34] and, thus, this technique is employed here. To the best of our knowledge experimental results concerning the molecular dynamics, crystallization behavior and thermal transitions (glass transition), demonstrating the changes from OEGMAs to comb-like POEGMAs with very short PEG chains, have not been reported yet. More specifically, we investigate the crystallization, glass transition and molecular dynamics of linear OEGMA with short (degree of polymerization, $d_p = 8$–9) or longer ($d_p = 19$) chains in parallel with comb-like POEGMAs consisting of short or long OEGMA branches (*i.e.* totally four compositions). For this work, we employ differential scanning calorimetry (DSC), of the conventional as well as the temperature-modulation mode (TMDSC), and broadband dielectric relaxation spectroscopy (BDS), supplemented by another special dielectric technique in the temperature domain, thermally stimulated depolarization currents (TSDC). Emphasis is given also on memory effects recorded on the crystallization behaviour of both the oligomers and the brush copolymers, where inter-chain interactions and structural constraints are expected to play a dominant role. The systems are studied upon equilibration unde room conditions (temperature and humidity), upon subjection to different melting/crystallization conditions and, especially for molecular dynamics, upon mild drying.

2. Materials and methods

2.1. Materials and synthesis

Four samples are studied here, shown schematically in Scheme 1, namely two commercial linear OEGMAs (Sigma-Aldrich) with short (475 g mol^{-1}, d_p = 8–9, ~4 nm, OEGMA-short)[35] and long (950 g mol^{-1}, d_p = 19 ~8 nm, OEGMA-long) chains and two comb-like polymers, POEGMA-short and POEGMA-long, consisting of 10 branches on average, that are the linear OEGMA-short and OEGMA-long, respectively. The POEGMAs were synthesized using the abovementioned short and long oligomers *via* the reversible addition–fragmentation chain transfer (RAFT) polymerization process (Scheme 2). It should be noted that PMMA/PEG polymer blends are reported to be miscible above the T_m for PEG,[15] therefore, the main and side chains in these graft copolymers are expected to be molecularly homogeneous when PEG is melted.

The OEGMAs were purified by mixing with inhibitor remover resins (Aldrich #311332), *via* stirring for 5 min, and subsequently the inhibitor remover resins were removed by filtration.

In order to prepare POEGMA polymers with short[35] and long side chains, reversible addition fragmentation chain transfer polymerization (RAFT polymerization) was employed, using 4-cyano-4-(phenylcarbonothioylthio)pentanoic acid (CPAD) as the chain transfer agent (CTA), 2,2-azobis(isobutyronitrile) (AIBN) as the radical source, to a CTA to initiator ratio ([CTA]$_0$/[I]$_0$) of 5 : 1 and 1,4-dioxane as the polymerization solvent. Before the polymerization reaction, the OEGMA monomers (M_n = 475 g mol^{-1} and M_n = 950 g mol^{-1}) were purified using a filled column including inhibitor removers (butylated hydroxytoluene and hydroquinone monomethyl ether, obtained from Sigma-Aldrich). AIBN was purified by recrystallization from methanol, CTA was used as received (Sigma-Aldrich) and 1,4-dioxane (99.8%) was dried over molecular sieves. The reaction was carried out for 24 h, under an inert atmosphere, at 70 °C (Scheme 2). After the polymerization, the reaction was quenched by cooling the solution at low temperature (−20 °C) and upon exposure to air. The resulting polymers were purified by precipitation in *n*-hexane excess twice. In the case of POEGMA-long, further purification was required, hence it was dialyzed against distilled water using a dialysis tubing cellulose membrane of 3500 Da MWCO to remove unreacted oligomer. The polymers were dried in a vacuum oven for 48 h at room temperature and then size exclusion chromatography (SEC) was implemented to determine the average molecular weights and molecular weight distributions.

All samples were studied mainly as received (ambient conditions), whereas in selected cases they were studied upon further drying. The latter was achieved by letting the sample to equilibrate at a low relative humidity of ~2 rh%, over phosphorus pentoxide (P$_2$O$_5$) in a sealed glass desiccator.

The main structural characteristics of the samples under investigation are listed in Table 1.

## 2.2. Characterization methods

2.2.1. Differential scanning calorimetry (DSC, TMDSC). The glass transition, crystallization and melting transition of the materials were investigated in a high purity helium (99.9995%) atmosphere in the temperature range from −150 to 70 °C by means of a TA Q200 series DSC instrument (TA Instruments, USA), calibrated with sapphires (for heat capacity) and indium (for temperature and enthalpy). The samples of the liquid-like form of ~8 mg in mass were closed in TZero aluminium pans and sealed with TZero Hermetic lids.

Totally three (3) thermal protocols for conventional DSC were applied and are described in the following: (*scan 1, partial melting for some samples*) Cooling from 40 °C to −140 °C at 10 K min^{-1} and heating to 70 °C at 10 K min^{-1}, (*scan 2, well melting*) cooling from 70 °C to −140 °C at 10 K min^{-1} and heating to 70 °C at 10 K min^{-1}, (*scan 3, isothermal annealing above melting*) melting of the samples for 10 min at different temperatures (*e.g.* 0–40 K) above their melting temperature, cooling to −150 °C at 10 K min^{-1} and subsequent heating at 10 K min^{-1}. The measurements indicated as *scan 3* aimed at the study of melt memory effects in the polymers of this work. Finally, all samples were investigated by DSC of the Temperature-Modulation mode[37] (TMDSC) with a heating rate of 2 K min^{-1}, a temperature amplitude of 1 K, and a modulation period of 60 s, in the temperature range from −140 to 40 °C, on fresh samples of ~12 mg in mass placed into Tzero aluminium TA pans.
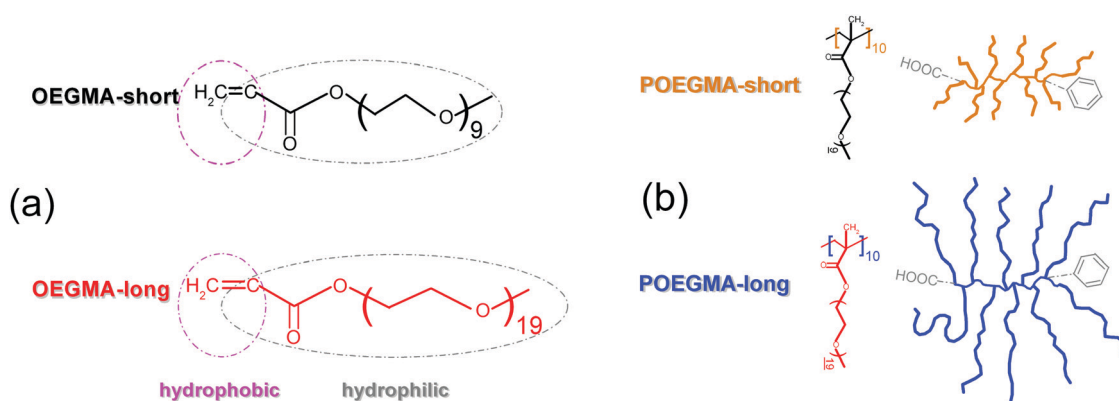
Scheme 1 Structure of the systems under investigation, namely (a) the linear oligomers OEGMA-short and OEGMA-long and (b) the corresponding comb-like polymers POEGMA-short and POEGMA-long.
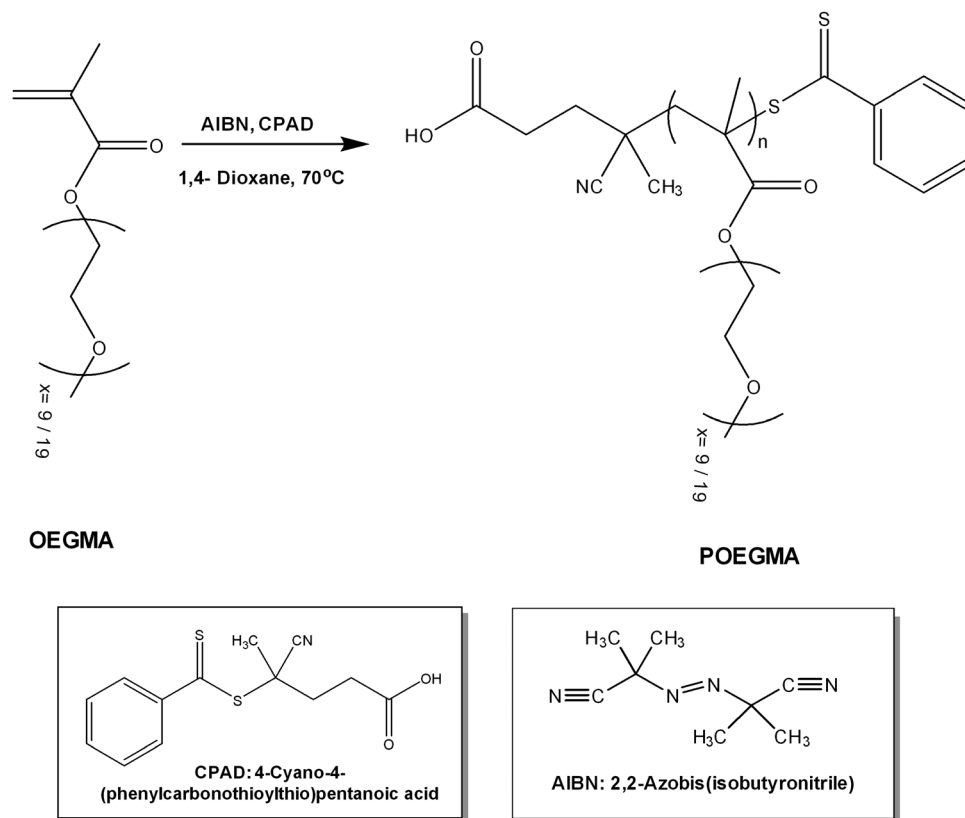
Scheme 2 Synthesis route for poly(oligo ethylene glycol methacrylate) *via* RAFT polymerization (POEGMA short $x = 9$, POEGMA long $x = 19$).

Table 1 Values of interest from the DSC measurements regarding scan 1, scan 2 and TMDSC: glass transition temperature, T_g, heat capacity change during glass transition, Δc_p, crystallization temperature and enthalpy, T_c and ΔH_c, respectively, crystalline fraction estimated from ΔH_c and comparison with the heat of fusion of poly(ethylene glycol) (197 J g^{-1})[36] and melting temperature and enthalpy, T_m and ΔH_m, respectively. Included are values for the average molecular weight, M_w, and the length of OEGMA (or side-chain/branch in POEGMA), L_{chain}[35]

Sample	M_w (g mol^{-1})	L_{chain} (nm)	Scan 1 T_g (°C)	Δc_p (J g^{-1} K^{-1})	Scan 2 T_g (K)	Δc_p (J g^{-1} K^{-1})	T_c (°C)	ΔH_c (J g^{-1})	CF$_{PEG}$ (wt)	T_m (°C)	ΔH_m (J g^{-1})	TMDSC T_g (°C)	Δc_p (J g^{-1} K^{-1})
OEGMA-short	475	3.9	−91	0.16	−91	0.17	−24	58	0.30	−31/−7	52	−90	0.22
OEGMA-long	950	∼8	−71	0.13	−70	0.13	19	104	0.53	34	107	−73	0.16
POEGMA-long	9500	∼8	−61	0.24	—	—	−4	93	0.47	36	106	−63	0.19
POEGMA-short	5000	3.9	−70	0.89	−70	0.89	—	0	0	—	0	−69	0.85

2.2.2. Broadband dielectric spectroscopy (BDS). BDS[30] measurements were carried out in a nitrogen atmosphere on liquid and liquid-like samples by placing them between finely polished brass plates of a capacitor (electrodes, 20 mm in diameter) employing thin silica spacers (∼50 μm in thickness), to keep the distance between the brass electrodes constant and ensure good electrical contacts. The capacitor was inserted between the parallel electrodes of a Novocontrol BDS1200 sample cell and an alternate voltage was applied to the capacitor in the sample cell. The complex dielectric permittivity $\varepsilon^* = \varepsilon' - i\varepsilon''$ was recorded isothermally as a function of frequency in the broad range from 10^{-1} to 10^6 Hz *via* a Novocontrol Alpha frequency response analyzer, at temperatures from −150 to 70 °C on heating,

at steps of 2.5, 5 and 10 K, depending on the process under investigation. Two temperature scans were performed. The temperature was controlled to better than 0.5 K with a Novocontrol Quatro cryosystem. Prior to the 1st BDS temperature scan the sample was cooled from room temperature (∼15–20 °C, *i.e.* partial melting) to −150 °C at 2 K min^{-1}, whereas prior to the 2nd BDS scan the sample suffered an isothermal annealing at 70 °C (well above melting) for ∼20 min and cooled to −150 °C at 2 K min^{-1}. Simultaneously with these cooling scans (ramps) ε^* was recorded for the selected high frequency of 100 kHz.

BDS results were analyzed by fitting model functions[30,38] to the experimental data in order to evaluate the time scale (temperature dependence of the frequency maxima of dielectric

loss), the dielectric strength and the shape parameters of the recorded relaxations.[30] To that aim, we employed the Havriliak–Negami (HN) equation[39]

$$\varepsilon''(f) = \varepsilon_\infty + \frac{\Delta\varepsilon}{[1 + (if/f_0)^{\alpha_{HN}}]^{\beta_{HN}}} \quad (1)$$

wherein, $\Delta\varepsilon$ is the dielectric strength, f_0 is a characteristic frequency related to the frequency of the maximum dielectric loss (ε''), ε_∞ describes the value of the real part of dielectric permittivity, ε', for $f \gg f_0$, and β_{HN} and α_{HN} are the shape parameters of the relaxation.[39] A sum of HN terms of type (1), one for each of the relaxations, was critically fitted to the experimental data at each temperature and the fitting parameters were determined. The temperature dependence of segmental dynamics (α relaxation) is typically described by the Vogel–Fulcher–Tammann–Hesse (VFTH)[30] equation, eqn (2),

$$f = f_0 \exp\left(-\frac{DT_0}{T - T_0}\right) \quad (2)$$

where T_0 is the Vogel temperature, D is the fragility strength parameter and f_0 is a frequency constant. In the case of local (non cooperative) dynamics, the corresponding temperature dependence obeys the Arrhenius equation,[30] eqn (3).

$$f(T) = f_{0,Arrh} \exp\left(-\frac{E_{act}}{kT}\right) \quad (3)$$

In eqn (3), E_{act} is the activation energy of the relaxation process and $f_{0,Arrh}$ is a frequency constant.

2.2.3. Thermally stimulated depolarization current (TSDC). TSDC is a special dielectric technique in the temperature domain[40] characterized by high sensitivity and high resolving power, the latter arising from its low equivalent frequency (10^{-4}–10^{-2} Hz). TSDC measurements were carried out in a TSDC Novocontrol setup (Novocontrol GmbH, Germany) on similar sandwich-like capacitors ($\sim$50 μm thickness and 20 mm in diameter) to those described above for the BDS measurements. The sample-capacitor was inserted between the electrodes (polished brass plates), placed in a Novocontrol TSDC sample cell and polarized by an electrostatic field E_p ($\sim$200 V μm^{-1}) at polarization temperature T_p for time $t_p = 300$ s. With the field still applied, the sample was cooled down to -150 °C (cooling rate 10 K min^{-1}, under nitrogen flow), sufficiently low to prevent depolarization by thermal energy, then short-circuited and reheated up to 30 °C at a constant heating rate, $b = 3$ K min^{-1}. Temperature was controlled to better than 0.5 K by means of a Novocontrol Quatro liquid nitrogen cryosystem. The discharge currents generated during heating were measured as a function of temperature with a programmable Keithley 6517B electrometer of high sensitivity.

3. Results and discussion

3.1. Crystallization and glass transition – calorimetry

Fig. 1 shows the DSC thermograms of scan 2, *i.e.* cooling from 70 °C to -140 °C at 10 K min^{-1} and heating to 70 °C at 10 K min^{-1}, during heating and cooling for OEGMA-short and OEGMA-long. Both samples exhibit crystallization (exothermic peaks) during

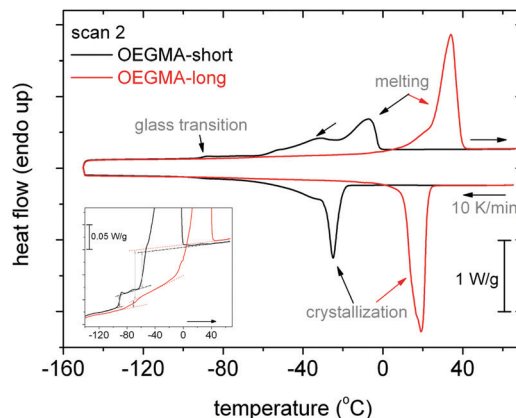**Fig. 1** Comparative DSC thermograms during cooling at 10 K min^{-1} and subsequent heating at 10 K min^{-1} of scan 2 (well melted samples) for OEGMA-short and OEGMA-long chains. The inset focuses on the glass transition during heating. The main thermal events are marked in the plots, whereas the heat flow (in mW) has been normalized to the sample mass (W g^{-1}).

cooling and glass transition (step) and melting (endothermic peaks) during heating. The respective characteristic values by DSC can be found in Table 1.

OEGMA-short crystallizes at $T_c = -24$ °C, exhibits a glass transition at a remarkable very low temperature, $T_g \sim -91$ °C, and complex melting peaks between -60 and -2 °C, with the maxima being located at $T_{m1} = -31$ °C and $T_{m2} = -7$ °C. The enthalpy of crystallization, ΔH_c, is equal to 58 J g^{-1}. To make an estimation of the crystalline fraction, CF, we compare ΔH_c with the enthalpy of fusion of a known polymer with the more similar structure to that of OEGMA, namely PEG, with $\Delta H_{PEG} = 197$ J g^{-1}.[36] We may report that in the literature different ΔH_{PEG} values have been used, for example 188 J g^{-1} [8] (and references therein), being however in a similar range to the value employed here. Thus, the crystalline fraction of OEGMA-short is estimated based on PEG to equal CF$_{PEG} = 0.30$ wt (Table 1). In the inset to Fig. 1, the glass transition step of OEGMA-short is quite sharp and demonstrates an overshoot at the high-temperature side. Such overshoots are generally observed for flexible chains (polymers) and have been correlated with structural relaxation.[41] These characteristics along the low T_g, in general, denote the expected enhanced mobility for OEGMA-short chains in the glassy state.[42]

On the other hand, the OEGMA-long chain (Fig. 1) crystallizes at the significantly elevated temperature $T_c = 19$ °C, *i.e.* more than 40 K higher than that of OEGMA-short. It should be marked that the latter T_c value is highly suppressed as compared to that of linear PEO chains.[6] OEGMA-long demonstrates a larger degree of crystallinity, equal to CF$_{PEG} = 0.53$ wt (Table 1). Then, T_g of OEGMA-long is -70 °C, *i.e.* by 21 K higher than that of OEGMA-short, accompanied by a quite more broad range of relaxation times, as reflected in the wide glass transition step. At higher temperatures, $\sim$34 °C (Fig. 1), the melting of crystals is recorded for OEGMA-long, which is $\sim$40 K higher than OEGMA-short.

The first clear effect recorded by DSC is that of the additive contribution of linear chain length on the degree (CF$_{PEG}$ increases) as well as the nucleation (T_c elevates) of crystallinity.

The increased T_g in OEGMA-long should be the combined result of the longer chain length[43] (according to the Fox-Flory prediction of MW dependence of T_g) and that of the increased crystallinity,[44] with the second factor expected to impose the most serious constraints on the amorphous chain diffusion.

The focus in now turned on the thermal transitions of the comb-like polymers *via* Fig. 2. Therein, the cooling/heating DSC scans for the two POEGMAs are comparatively shown with those for OEGMAs. In Fig. 2a, POEGMA-long exhibits a single crystallization peak at $-4\ °C$, *i.e.* 23 K lower than its homologue oligomer OEGMA-long, and melting at $\sim 36\ °C$. Surprisingly, we cannot distinguish a clear glass transition step in Fig. 2b for PEOGMA-long during scan 2 despite the fact that CF_{PEG} equals 0.47 wt, being smaller than that of the corresponding oligomer. Interestingly, when looking back at the results for scan 1 for the same sample (dashed–dotted line in Fig. 2b), a clear glass transition step is revealed at $-61\ °C$ (Table 1). We recall that the only difference between the measurements of scan 1 and scan 2 is that of the different initial temperature prior to the cooling, namely, $40\ °C$ and $70\ °C$ for scan 1 and scan 2, respectively. A full

temperature range comparison between scans 1 and 2 (as well as upon fast cooling) can be found in Fig. S1 in the ESI.† Therein, the difference in the initial temperature, from 40 to 70 °C, had resulted also in a significant change in T_c, namely from 21 to $-4\ °C$, respectively. We will come back to this interesting point in the next section (melt memory effect).

Coming to POEGMA-short in Fig. 2, the sample demonstrates a completely amorphous character, as neither crystallization nor melting peaks are recorded. Instead, a strong glass transition step at $T_g = -70\ °C$ with a large change in heat capacity $\Delta c_p = 0.89\ J\ g^{-1}$ is recorded as the unique thermal transition of POEGMA-short. The values are identical for scans 1–3 (not shown) denoting independency of the glass transition from the initial temperature and the cooling rate, in contrast to POEGMA-long. The values for the T_g and Δc_p have been checked also by the more advanced technique of TMDSC (Fig. 2c) and were found to be similar to those by the conventional DSC (Table 1). Interestingly, the recorded value of Δc_p for the fully amorphous POEGMA-short is in perfect agreement with the Δc_p value calculated for the amorphous PEG chains of the brush
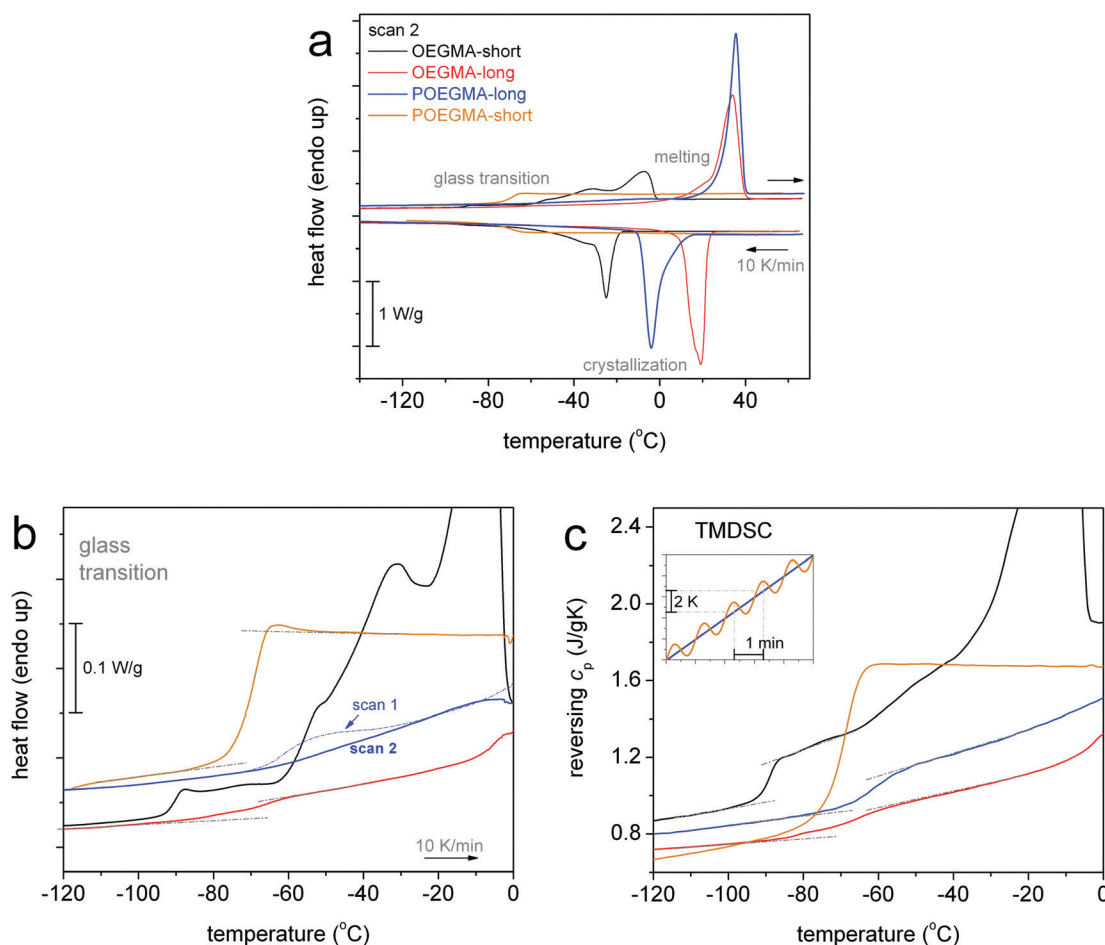
Fig. 2 (a and b) Comparative DSC thermograms of scan 2, namely, during cooling at 10 K min^{-1} and subsequent heating at 10 K min^{-1} (well melted samples) for all samples studied (OEGMAs and POEGMAs) in (a) the overall temperature range and (b) the glass transition temperature region. The main thermal events are marked in the plots, whereas the heat flow (in mW) has been normalized to the sample mass (W g^{-1}). The results for scan 1 for OEGMA-long have been added in b (dashed–dotted line) for comparison. (c) The corresponding results by TMDSC in the glass transition temperature region in the form of the reversing part of heat capacity.

polymer taking into account the value that has been suggested for fully amorphous PEO (0.97 J g^{-1} K^{-1})[45] and the weight fraction of PEG side chains in the POEGMA-short macromolecule ($\sim$0.82 wt).

Combining all results on crystallization together up to this point, we conclude to Fig. 3. In Fig. 3a, it becomes clear that by doubling the length of linear OEGMAs from $\sim$4 to $\sim$8 nm both the T_c and CF$_{PEG}$ increase, indicating that the number of crystal nuclei increases and, most probably, the thickness of the crystalline lamella, as is also suggested by the simultaneous increase of T_m (Fig. 3b). Nucleation seems to be hindered when going from linear OEGMA-long to comb-like POEGMA-long, as T_c decreases along with CF$_{PEG}$. At the same time T_m seems to be almost unchanged in Fig. 3b. The effect can be rationalized considering the different morphologies of the two samples (inset schemes in Fig. 3a) and, consequently, the different constraints imposed on the spatial distribution of the polymer chains and their packing manners, along with the impact of these morphologies on the expected inter-chain interactions (polar interactions) between the OEGMA chains.[2] Coming to POEGMA-short, again on the basis of the schematic scenario of Fig. 3a, we propose that the short-branched comb entities of POEGMA-short preclude the formation of similar lamellar packing, in contrast to the rest of the cases, including that of OEGMA-short. In addition, in the case of POEGMA-short we could conclude that either no nucleation takes place, due to quite a small number of initial contact points, or that the crystallizable chains fail to be integrated into growing crystals due to significant geometrical constraints.[14]

3.2. Melt memory effects in crystallization behavior

Previously we commented on the different T_c between the semicrystalline samples and the effect of the cooling rate for a given sample; more interestingly, on the effect of different initial temperatures, $T_{initial}$, above T_m (40 °C for scan 1 and 70 °C for scan 2) on the T_c for POEGMA-long. Looking back to the data for all semicrystalline samples and comparing between scans 1 and 2, we observed similar behaviors.

To follow further this phenomenon, we performed for all semicrystalline samples further DSC measurements (scans 3), namely by increasing gradually $T_{initial}$ by 5 K (always in the molten state), performing 10 min isothermal annealing there, and cooling to −150 °C at 10 K min^{-1}. For POEGMA-long, we additionally performed a 30 min isothermal annealing at 17 °C, i.e. below its melting point and almost at the onset of its crystallization (melt- or hot-crystallization annealing). The results by these measurements are shown in Fig. 4–6.

Fig. 4 shows the results by scans 3 for the two linear oligomers. In both cases the elevation of $T_{initial}$ results in the significant lowering of T_c by up to 11 K for OEGMA-short and 12 K for OEGMA-long (vertical double arrows in Fig. 5). At the same time CF$_{PEG}$ remains unchanged and T_m decreases by a few K. This effect can be understood by invoking the concept of annealing in a non-isotropic melt and subsequent recrystallization of the semi-crystalline polymers *via* the self-nucleation mechanism (melt memory effect). Annealing at $T_{initial}$ ($T_{initial}$ being close to, however, above the melting peak in DSC scans) the thermal history of the sample is not completely erased and the recrystallization during cooling is accelerated *via* a self-nucleation process. The lower the value of $T_{initial}$, the higher the T_c upon cooling from the annealing stage, indicating a stronger nucleation effect.[22,24] Thus, the observed suppressions in T_c with an increase in the annealing temperature denote the retarded self-nucleation process that, in our case, may be correlated with the inter-chain interactions and chain–chain associations.[22,26] With increasing $T_{initial}$ above T_m, the linear OEGMA chains seem to be gradually dissociated from each other (inset schemes in Fig. 4 and 6), revealing, thus, a structured molten state. The crystallization behavior of the oligomers is more clearly shown in Fig. 5, where the heating DSC scans of the oligomers (scan 2) are plotted together with the T_c values recorded during cooling after annealing for 10 min at various temperatures ($T_{initial}$, in scan 3). The data of $T_{initial}$ in Fig. 5 are in the so-called self-nucleation domain, i.e. $T_{initial}$ is at temperatures where the endothermic melting peak completely disappears in the DSC heating scan.[22,27] We observe that for OEGMA-long the thermal history is erased by annealing at
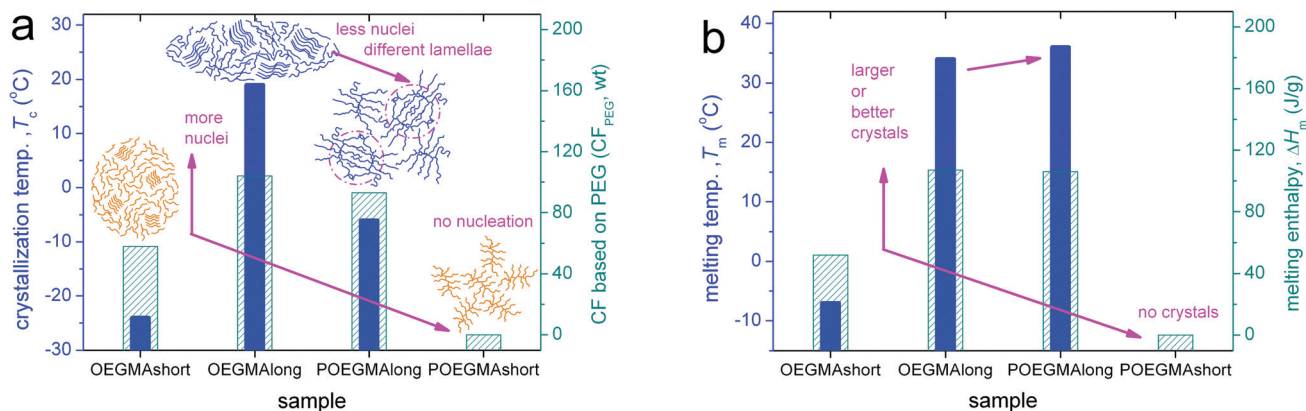

Fig. 3 Column diagrams comparing (a) T_c with CF and (b) T_m with ΔH_m for all samples. The insets to (a) are simplified models employed here to rationalize the observed changes in crystallization (arrows) arising from the length of the OEGMA branch and the change from linear oligomers to the comb-like polymers.
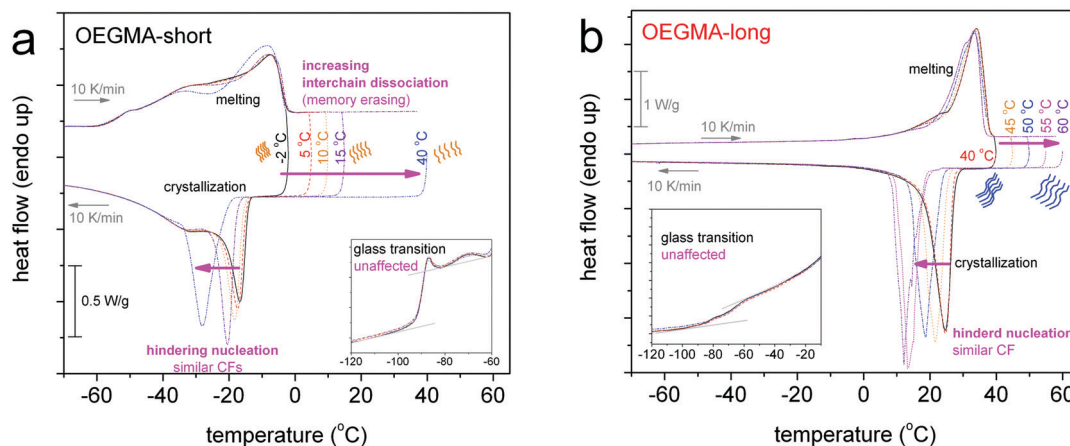
Fig. 4 DSC cooling/heating thermograms for (a) OEGMA-short and (b) OEGMA-long, revealing the effect on crystallization by isothermal annealing (10 min, scans 3) at gradually higher temperatures above $T_{\rm m}$. The results can be rationalized via the inset schemes, namely, by respective increase in chain–chain dissociations (melt memory effects).
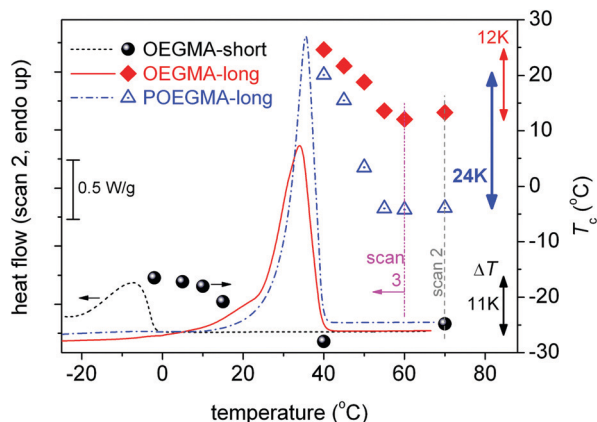

Fig. 5 (Left axis, lines) Heating DSC scans of the two linear OEGMAs and POEGMA-long recorded during the scan 2 protocol and (right axis, points) the corresponding crystallization temperatures, T_c, as a function of $T_{\rm initial}$ superimposed on the melting endotherm of each sample (data obtained by scan 3). Included are also the T_c recorded during cooling in scan 2 (vertical short-dashed line), i.e. starting cooling at 70 °C after annealing there for 1 min.

temperatures of about 20 K above the end of the melting event, whereas, interestingly, for OEGMA-short the corresponding critical temperature elevation seems to be higher than 20 K in Fig. 5. The strength of the melt-memory effect can be indicated by the maximum recorded value of $\Delta T = T_c - T_{\rm c,isomelt}$, where T_c is the value recorded in scan 3 measurements and $T_{\rm c,isomelt}$ the saturated value of T_c when the sample is cooled from its isotropic melt, i.e. with no "memory structure".[22,27] The data in Fig. 5 suggest that melt-memory effects are of comparable strength in the oligomers.

Since $T_{\rm m}$ does not change significantly and, furthermore, glass transition is also unchanged (neither in the position nor in strength, insets to Fig. 4), we expect similar semicrystalline morphology, namely in the size, number, and distribution of crystals,[46–48] for different $T_{\rm initial}$.

The situation in the semicrystalline comb-like polymer POEGMA-long (Fig. 6) is even more interesting. The increase

of $T_{\rm initial}$ up to 45 °C leads to similar effects to that in the linear oligomers. For a further increase in $T_{\rm initial}$ to 50 and 55 °C, T_c drops rapidly to 3 and −4 °C, respectively. The phenomenon does not proceed with a further increase in $T_{\rm initial}$ to be 60 and 70 °C, suggesting that 55 °C is the lower temperature for complete chain–chain dissociation (Fig. 5). In other words, for the comb-like POEGMA-long 55 °C is the lower temperature for fully erasing the sample's structure memory in the melt. Furthermore, although the critical temperature for erasing thermal history in POEGMA-long is only 15 K above the melting event, i.e. lower than in OEGMA-long (please see Fig. 5), the strength of the melt-memory effect as indicated by the maximum of $\Delta T = T_c - T_{\rm c,isomelt}$ is double than in the linear homopolymer (about 24 K, a vertical double arrow in Fig. 5). These features imply that due to complex topological constraints existing in the brush polymers, different mechanisms may drive the memory effect between the linear and comb-like polymer architectures. Simultaneously, for $T_{\rm initial} \geq 55$ °C, $T_{\rm m}$ decreases slightly, the melting profile exhibits a qualitative change and $CF_{\rm PEG}$ remains almost unchanged. Nevertheless, the glass transition vanishes in Fig. 6b, indicating in this case that the semicrystalline morphology is severely altered, leading to more serious constraints on the mobility of the amorphous polymer fraction. A final point with respect to the data of Fig. 5 refers to the width of the region wherein the T_c changes with $T_{\rm initial}$. Based on the self-nucleation theory,[49] the said region is called the 'self-nucleation domain (DII)'.[22] The self nucleation domain is wider for OEGMA-short, whereas more short in the case of longer OEGMA and POEGMA.

More work is needed, for example, by wide angle X-ray scattering (WAXS) to identify the proposed alternations in the crystal structure as well as by small angle X-ray scattering (SAXS) for the presence of large nanoscopic domains due to the amphiphilic character of the OEGMAs. Regarding the suggested alternation in the semicrystalline morphology between the different samples or between the different thermal protocols for the same sample, polarized light microscopy (PLM) measurements,[50] again at low temperatures, could shed more light.
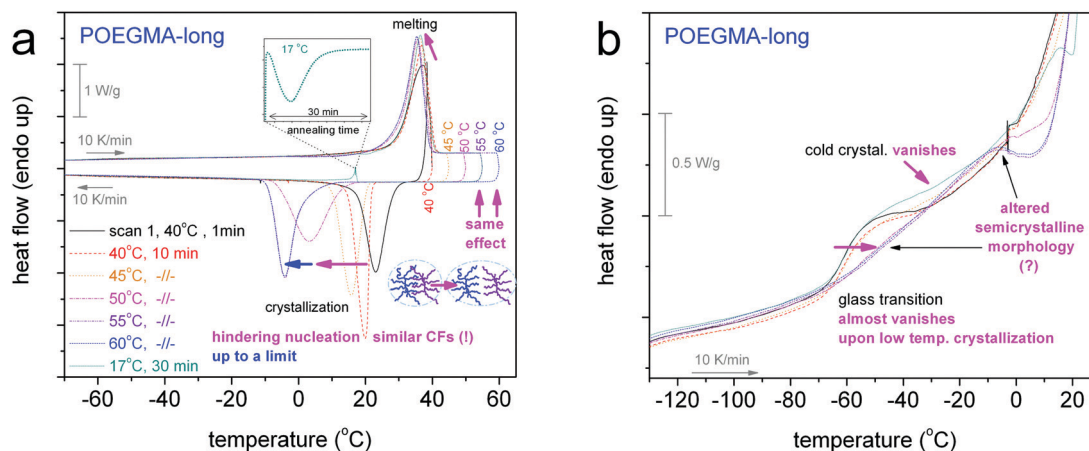
Fig. 6 (a) DSC cooling/heating thermograms for POEGMA-long demonstrating the strong memory effects on crystallization, by 10 min isothermal annealing at gradually higher temperatures above T_m and, in contrast, by 30 min isothermal annealing at a temperature below T_m (17 °C, inset to a). The inset schemes are used for rationalizing the results *via* the degree of inter-chain associations/dissociations. (b) Focus on the interesting behaviour of glass transition, arising from the prior thermal (crystallization) treatments, details being given in the main text.

3.3. Molecular dynamics – dielectric spectroscopy

Raw BDS results. The results by BDS for each sample are presented in Fig. S2 in the ESI,† in the form of isothermal curves of the imaginary part of dielectric permittivity, ε'', against frequency, f, for all temperatures of recording. Additional raw data by BDS can also be found in Section S2 in the ESI.† Totally five relaxation processes related to molecular mobility are recorded in the light of BDS.

To more easily follow the temperature evolution of the ε'' isotherms, data from Fig. S2 (ESI†) for selected temperatures both below and above T_g are reproduced in Fig. 7 and shown comparatively for all samples. Along with these data we added results by the employed fitting of $\varepsilon''(f)$ peaks in terms of HN models (HN, eqn (1), Section 2.2.3) for POEGMA-long and OEGMA-long.

At temperatures lower than the T_g, we record for all samples the secondary γ and weak β relaxation (Fig. 7a and b), whereas at temperatures above T_g we record the segmental α (Fig. 7c and d) relaxation which is the dielectric analogue of the calorimetric glass transition.[30] In the case of linear OEGMAs, an additional quite strong process is recorded closely to α, however at lower frequencies. This is the case of the slightly slower process α' in Fig. 7c and d. For a further increase of the temperature, the frequency response signal is dominated, especially at the low-f side, by strong phenomena related to ionic conductivity (electrical carrier motion, σ peak) and, possibly, interfacial polarization effects.[30]

The various effects in molecular dynamics will be discussed in the next section on the basis of comparative dielectric maps (Arrhenius plots) determined *via* the employed fitting. The parameters of fitting as well as additional evaluation, namely the activation energy, E_{act}, of local relaxations, the fragility (or else cooperativity) index, m,[51] and the dielectrically estimated glass transition temperature, $T_{g,diel}$ (extrapolated time scale of α at the relaxation time $\tau = 100$ s)[30] are listed in Table 2 for all samples.

Overall dielectric-calorimetric dynamics map. We now come to the overall dielectric map of Fig. 8a, wherein we present the

reciprocal temperature dependence of the relaxation time τ corresponding to the ε'' maxima (peaks). For the sake of clarity, we separated the results to those for the linear oligomers (Fig. 8a – top) and for the comb-like polymers (Fig. 8a – bottom). Included in the dielectric map are points by DSC (for T_g) and by the special dielectric technique in the temperature domain, TSDC, at the corresponding equivalent relaxation times TSDC. In Fig. 8b we show the respective results for the reciprocal temperature dependence of dielectric strength, $\Delta\varepsilon$.

Local γ relaxation. The γ process exhibits all the characteristics of a local polymer relaxation process, namely an Arrhenius-like time scale (linear) with constant E_{act} (0.3–0.4 eV, Table 2), a symmetric shape ($\beta_{HN} = 1$, Table 2) and an increasing $\Delta\varepsilon(T)$ trend (Fig. 8b). Putting the time-scale data together in a common diagram we created Fig. S6 (ESI†). Therein, γ for the POEGMAs, γ_{POEGMA}, is almost identical, whereas it is accelerated in the two OEGMAs, γ_{OEGMA}. Compared with the structurally similar polymer, PEG, in Fig. S6 (ESI†) the corresponding process, γ_{PEG},[52,53] fits quite well with γ_{POEGMA} here. γ_{PEG} has been attributed to the 'crankshaft motions' of methylene sequences.[54–56] In the case of POEGMA-long, γ_{POEGMA} demonstrates a change in its E_{act} (from 0.38 to 0.55 eV, Table 2) at higher temperatures. In a very recent work, Czaderna-Lekka *et al.*[28] studied by BDS several poly(oligo(ethylene glycol) methyl ether methacrylate) (POEGMEA) networks including samples with similar numbers of oxyethylene groups (8–19). They recorded a γ process with a similar time scale to that of γ_{POEGMA} here, slightly lower $E_{act} \sim 0.26$ eV (24.9 kJ mol^{-1}) and attributed its origins to the dipole moments of the ending methoxyl groups.[57–59]

Local β relaxation. The weak β process is described again by an Arrhenius-like (Fig. 8a) symmetric relaxation (Table 2) of a higher $E_{act} \sim 0.7$ eV (Table 2) and slower time-scale as compared to γ. This suggests that β is related to either larger molecular entities and/or of more difficult (constraint) mobility than γ. Similarly to γ, in Fig. 8a (please see also Fig. S6, ESI†) the points of β for the POEGMAs are more close to each other,
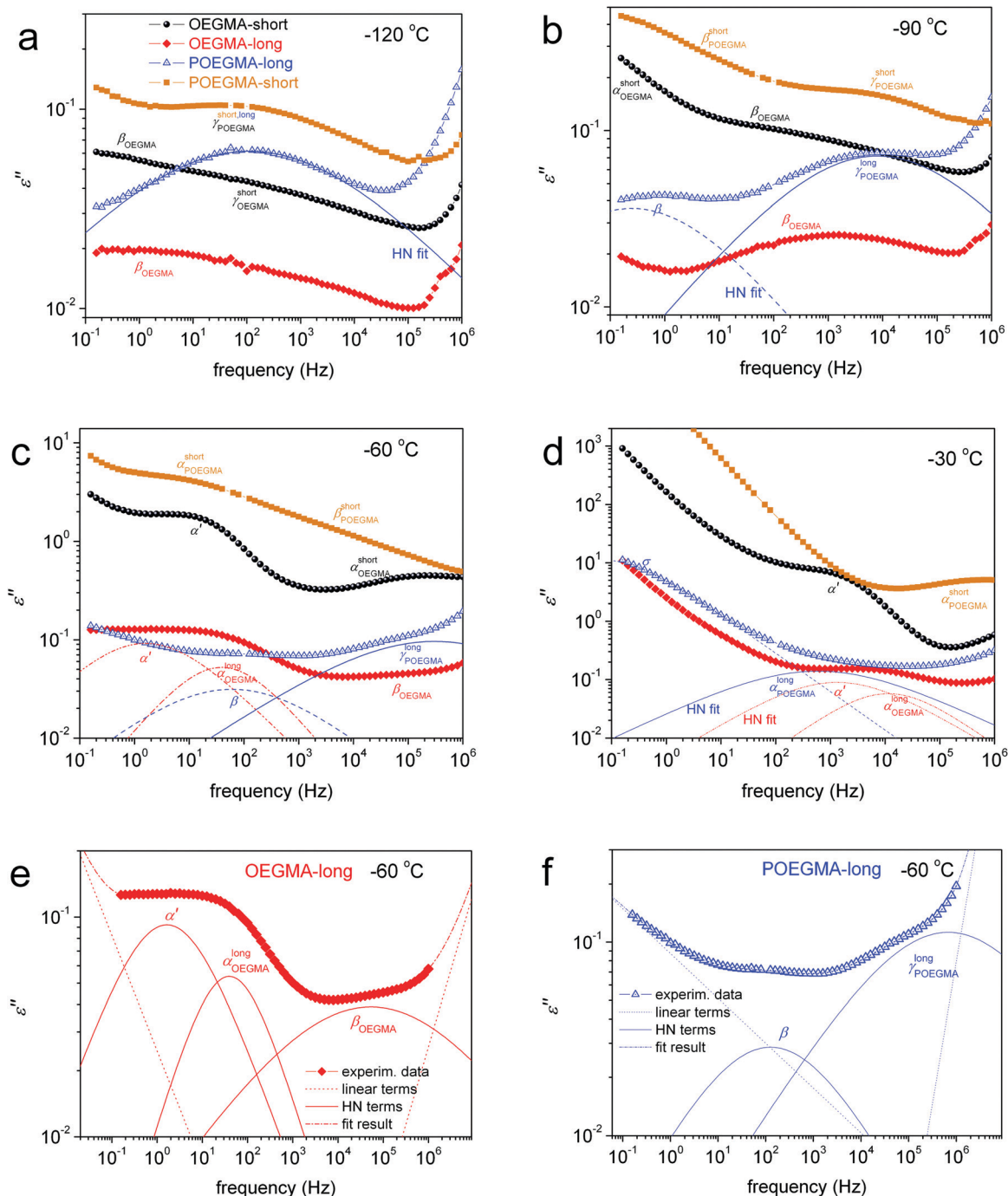
Fig. 7 Comparative isothermal BDS plots of ε'' against frequency for all samples (description in a), at the selected temperatures (a) -120 °C, (b) -90 °C, (c) -60 °C and (d) -30 °C. The recorded ε'' peaks are indicated on the plots. The added lines (solid and dashed–dotted) are examples of analysis by means of fitted Havriliak-Negami (HN) terms for POEGMA-long and OEGMA-long; full term analysis being shown in (e) and (f).

moreover, being separated (slower) from those of the OEGMAs (faster β therein). Comparing again with PEG we find slower β points for POEGMAs to coincide well with those for a relaxation of PEG assigned to hydrated local sites of the polymer chain ($\beta_{PEG,JG}$)[52,53] (and references therein). In Fig. S6 in the ESI,† we demonstrate the vanishing of β of POEGMA-long (under ambient conditions) upon drying (at ~ 2 rh% over P_2O_5), while, in our recent study[35] on the same POEGMA-short however

purposely dried therein, β was also absent. Therefore, we conclude that β relaxation here arises from the hydrophilic part of our amphiphilic OEGMA chains, and is triggered by the presence of water molecules. The E_{act} of β in PEG has been found to change at temperatures above T_g and due to that it has been addressed also as a relaxation of the Johari–Goldstein (JG)[60] type.[52,53] Such a change in the time scale is recorded here for β in OEGMA-short (Fig. 8a, E_{act} changes from 0.65 to ~ 1.00 eV,

Table 2 Values of interest from the analysis of the BDS measurements: shape parameters of the Havriliak–Negami (HN) equation, α_{HN} and β_{HN}, activation energy, E_{act} (in eV and kJ mol^{-1}, Arrhenius equation), fragility index for α relaxation, m_α, and dielectric glass transition temperature, $T_{g,diel}$ (details in the main text)

	γ Relaxation				β Relaxation				α Relaxation				α' Relaxation	
Sample	α_{HN}	β_{HN}	E_{act} (eV)	E_{act} (kJ mol^{-1})	α_{HN}	β_{HN}	E_{act} (eV)	E_{act} (kJ mol^{-1})	α_{HN}	β_{HN}	m_α	$T_{g,diel}$ (°C)	α_{HN}	β_{HN}
OEGMA-short	0.3	1	0.3	29	0.3	1	$0.65 \rightarrow 1.00^a$	$63 \rightarrow 96$	0.5	0.6	96	−92	0.8	1
OEGMA-long	0.3	1	0.31	30	0.3	1	0.68	66	0.7	1	141	−81	0.6	1
POEGMA-long	0.4	1	$0.38 \rightarrow 0.55^a$	$37 \rightarrow 53$	0.4	1	0.67	65	0.7	1	86	−53	—	—
POEGMA-short	0.3	1	0.33	32	0.4	1	$0.63 \rightarrow 1.8^a$	$61 \rightarrow 174$	0.4	0.5	96	−70	—	—

^{a} Changes with temperature that cannot be sufficiently represented by an average value.
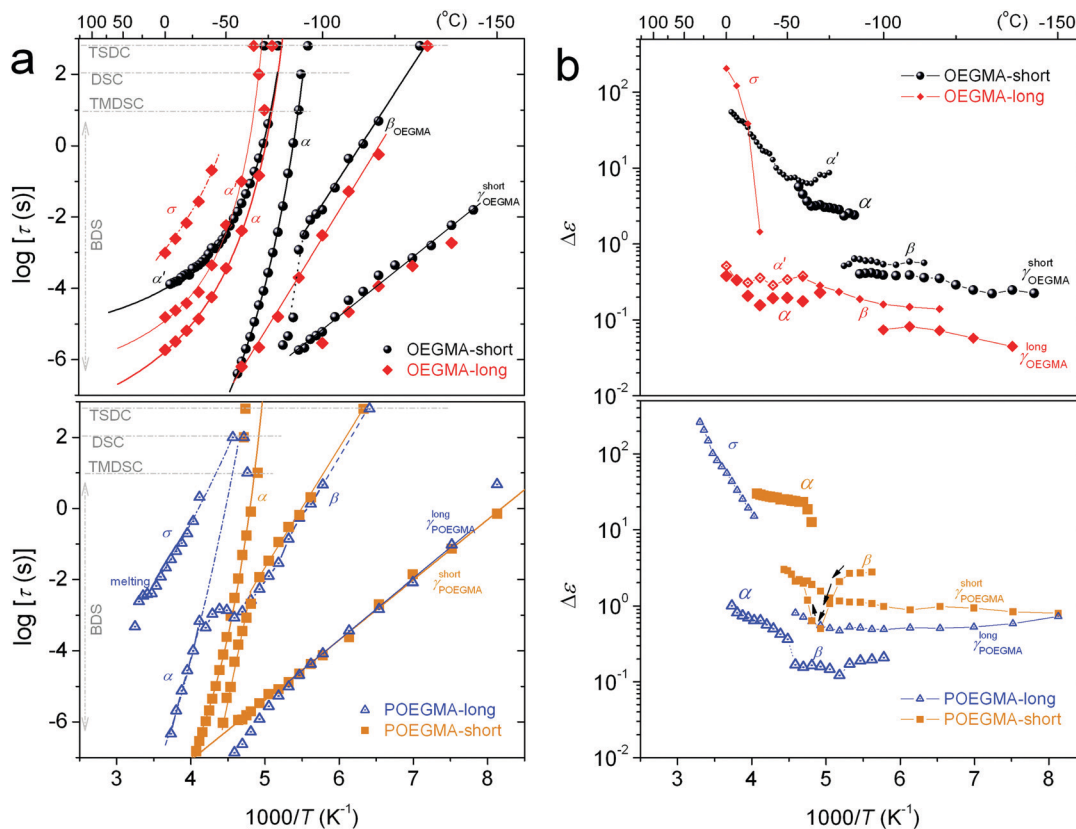
Fig. 8 (a) Dielectric-calorimetric map (Arrhenius plots) and (b) dielectric strength, $\Delta\varepsilon$, namely the reciprocal temperature dependence of the relaxation times (τ) and $\Delta\varepsilon$, of the various relaxations recorded for (top) the two linear oligomers and (bottom) the two comb-like polymers. The lines connecting the experimental points are fittings of the Arrhenius (straight lines) and the Vogel–Fulcher–Tammann–Hesse (curved lines). Included in (a) are data for the calorimetric T_gs (DSC, TMDSC) and results by TSDC at the corresponding equivalent relaxation times.

Table 2). In the recent work, Czaderna-Lekka et al.[28] reported a process of similar time-scale and strength to β here, exhibiting an increase in E_{act} with the increase in the oligoether chain length. Also, therein,[28] in the case of longer chains, β was found to be strongly affected by cold crystallization. We could not check such effects in our case as the E_{act} of β is almost identical for all samples (0.65–0.67 eV, Table 2) and cold crystallization is not recorded here, moreover, it cannot be recorded at temperatures below T_g.

Regarding local dynamics in general, it is clear that both types of processes are recorded faster in the linear oligomers. Considering the probable molecular origins for these dynamics

as described above we can rationalize this effect via the concept of less inter-molecular interactions in the OEGMAs and, on the other hand, of more geometrical constraints in the mobility of side chains in the comb-like POEGMAs. Consequently, we expect the γ and β processes to be activated, on the one hand, from the same molecular groups,[35] however, in the comb-like entities of POEGMA under more 'constraints'.

Segmental α relaxation. α relaxation arises from dipole moment components perpendicular to the chain backbone (Scheme 3, bottom right).[30] In Fig. 8a, the time scale of α obeys the VFTH law[61] (eqn (2), curved lines). When extrapolating the VFTH curves toward higher relaxation times in the dielectric
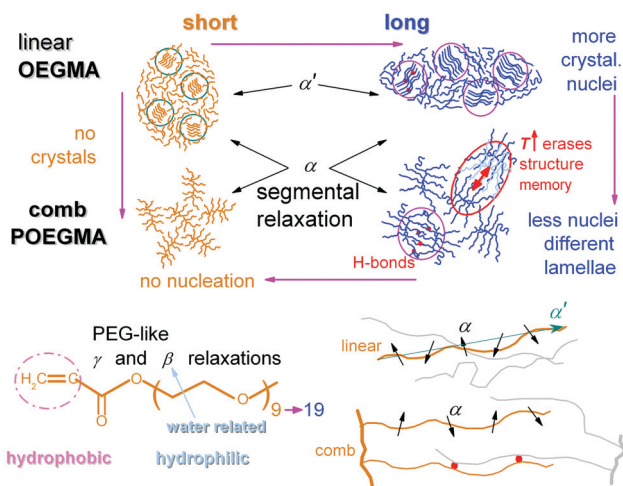
Scheme 3 Simplified model schemes for rationalizing the overall effects on crystallization (top) and describe the proposed origins of the segmental and local dynamics in the linear OEGMAs and comb-like POEGMAs (bottom).

map, the points of α meet quite well with those by DSC and TSDC. This proves that α is the dielectric analogue of glass transition. Regarding the shape of α, by taking a glance of Table 2 in the case of long chain-based systems the relaxation is symmetric with ($\alpha_{HN} \sim 0.7$, $\beta_{HN} = 1$) while for the short chain-based one the relaxation is asymmetric ($\alpha_{HN} \sim 0.4$–05, $\beta_{HN} = 0.4$–0.6). In POEGMA-short and OEGMA-short this can understood from the lower CF_{PEG} (0 and 0.30 wt, respectively Table 1) suggesting that molecular mobility is not seriously affected by the crystals for the linear chains.[30] In such a simple case, we would expect also that $\Delta\varepsilon$ decreases with T, which is the conventional behavior for an α process in amorphous polymers.[30] Actually, the opposite $\Delta\varepsilon(T)$ behavior can be followed in Fig. 8b, namely the $\Delta\varepsilon$ increasing with T. This suggests that serious constraints may already exist, even in the amorphous POEGMA-short; furthermore, the constraints are gradually loosened with temperature. As seen in Scheme 3, we can

imagine that such constraints can be in both cases the inter-chain interactions and, additionally, those imposed by the comb-like structure of OEGMA 'grafted' practically on an almost rigid backbone. Due to this grafting in addition to more forced inter-chain interactions in POEGMA-short we also record the α relaxation decelerated (slower, Fig. 8a and Fig. S6, ESI†) exhibiting lower cooperativity (fragility, $m_\alpha \sim 141$, Table 1) as compared to OEGMA-short ($m_\alpha \sim 92$). When comparing between short and long oligomers, in OEGMA-long α is symmetric, weaker, however, exhibits increased cooperativity than that of OEGMA-short. We recall that CF_{PEG} has become now more significant, 0.53 wt (Table 1), which is compatible with more retarded dynamics of the mobile amorphous segments. In the comb-like POEGMA-long, α is the most slow among the samples, it is again symmetric due to the high CF_{PEG} (0.47 wt) and demonstrates a moderate fragility ($m_\alpha = 86$). This experimental finding suggests that in POEGMA-long the segments that contribute to the α process exhibit more hindered dynamics, as compared to the linear oligomer, being 'grafted' onto the PMMA backbone of the comb (Scheme 3).

Segmental-like a' process. In the raw data of the BDS (Fig. 7c and d) for the two linear OEGMAs an additional process/peak (indicated as α') is recorded at some orders of frequency lower than α. This is in agreement with the TSDC results for the same samples (Fig. 9), moreover, upon employing the more advanced methodology of selected thermal sampling (i.e. selecting the activation temperature window).[62] More specifically, while the temperature position of α in TSDC (when recorded) for the different samples follows well that of T_g, the additional contribution of α' in the oligomers was further checked exploiting the more sophisticated technique of polarization within a selected temperature window, an example being shown for OEGMA-long in Fig. 9b. α' was found to arise from a real dipolar motion rather than being related to ionic conductivity. More results by TSDC, involving various polarization and thermal protocols, can be found in Section S3 in the ESI.†

The magnitude ($\Delta\varepsilon$) of α', in BDS measurements, lies on a similar order to that of α. α' was fitted with the HN equation,
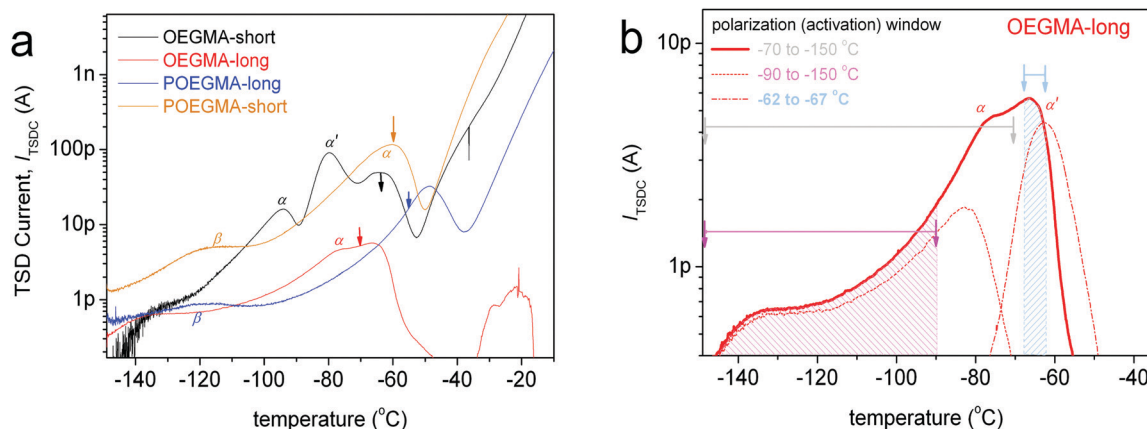
Fig. 9 (a) Comparative TSDC curves for all samples, for selected T_p, being indicated the main relaxation peaks recorded. (b) More advanced TSDC possibilities, in particular results for OEGMA-long comparing between the overall and partial temperature range polarization (thermal sampling) and revealing two discrete contributions (α and α') to the TSDC related to segmental dynamics.

giving the shape parameters $\alpha_{HN} \sim 0.6$–0.8 and $\beta_{HN} = 1$ (Table 2) which are indicative of a symmetric and quite narrow peak (similar to the corresponding TSDC peak in Fig. 9b). The results for the time scale of this process have been included in our dielectric maps. α' obeys the VFTH law, with however significantly different fragility as compared to α. The extrapolation of the VFTH curves to the equivalent DSC relaxation time (100 s) makes the process to approach the calorimetric T_g.

Combining all the above results we suspect that the dipolar and very narrow process α' might be the manifestation of the Normal Mode (NM) relaxation, hardly observed in PEG macromolecules due to enhanced crystallinity.[63–65] It is supposed that the particular molecular structure of OEGMAs, i.e. the amphiphilic nature of chains that have no "active" end-groups, may be the cause of the activation of the NM relaxation process, which arises from the fluctuation of the polymer chain end-to-end vector (parallel to the OEGMA chain, Scheme 3, bottom-right). Upon critical analysis such contribution could not be resolved for the POEGMAs. On the basis of Scheme 3 again, this can be understood via the one-side grafted OEGMA chains in the comb-like entities, which makes the 'global dipole' fluctuation quite more weak (very low $\Delta\varepsilon$).[65] Moreover, the one-side-grafted chain is expected to exhibit a faster NM, in particular, of ~ 4 times smaller relaxation time as compared to the corresponding free chain, due to the tethered chain end.[65,66] In this case, the NM here may demonstrate the same time scale as the segmental α relaxation. Similar processes have been recorded by Kozanecki et al.[29] in poly(2-(2-methoxyethoxy)ethyl methacrylate) and, more recently, by Czaderna-Lekka et al. in POEGMEA networks,[28] however they did not extensively discuss its behavior. For the time being, we wish to not further comment on the interpretation of α'.

At the higher temperature/lower frequency side of Fig. 7d and 8, the strong σ process is recorded. σ is exceptionally narrow ($\alpha_{HN} = 0.7$) and symmetric ($\beta_{HN} = 1$). σ is most probably related to long range charge transport through the amorphous regions and subsequent charge accumulation at interfaces in the semi-crystalline structures.[67] With an increase in temperature we observe in Fig. 8a (bottom) a disturbance in the time scale of σ, which is most probably the effect of melting of the crystals and restructuring of the morphology (please compare with Fig. 2a).

So far, the results of the present study could be interpreted by employing a combination of the existing knowledge, similar effects from the literature and schematic models developed in the frame of this investigation. From the methodological point of view, the widely used combination of the techniques here, DSC and BDS, were once again proved quite useful and effective in illuminating aspects regarding the molecular dynamics and possible structure, even at the nanoscopic scale. Obviously more work is needed to shed more light on specific raised questions, for example, with respect to the crystallization and structuring of the linear OEGMAs and comb-like POEGMAs. Measurements on these systems by wide/small angle X-ray scattering (WAXS/SAXS) in combination with Fourier transform infrared (FTIR) spectroscopy are expected to provide further insight, for example by the monitoring of crystal structuring, identification of probably ordered structures in larger domains and record changes of the inter- and intra-chain interactions. Also, PLM measurements under various conditions could be found useful for studying the semicrystalline morphology.

4. Conclusions

In this paper we show results on thermal transitions and molecular dynamics in new amphiphilic linear oligomers with short and longer chains, OEGMA (-short ~ 4 nm, -long ~ 8 nm), in direct comparison with their homologue comb-like polymers, POEGMAs (-short and -long), with ~ 10 OEGMA-branches. The investigation involved measurements by calorimetry (DSC) and dielectric spectroscopy (BDS, TSDC). With the exception of POEGMA-short, all samples are semicrystalline, with the amount of crystallinity (0 to 53 wt%) and the nucleation being favored (elevated T_c) for the longer chains. The semicrystalline systems exhibit also 'memory' characteristics related to the nucleation of crystals, the effect being more pronounced for the comb-like architecture. These results are rationalized in terms of the role of expected inter-chain interactions, namely hydrogen bonds, on the initial polymer ordering (nucleation) and further on crystal growth. The changes in T_g (-91 to -61 °C) seem to follow those of CF especially when the latter is high (>40 wt%). The direct chain length effects cannot be resolved here, as the samples cannot be kept in the amorphous state.

BDS in combination with TSDC enabled the molecular dynamics mapping of these systems for a wide temperature range (-150 to 50 °C). All samples demonstrated two sub-T_g local relaxations (γ and β), interestingly, resembling those of the more similar polymer, PEG. Especially β is a water-related process and arises from the hydrophilic part of OEGMA. The dielectric analogue of glass transition, α relaxation is recorded here for all samples, with its time scale being in close agreement between the three techniques. Obviously, α arises from the chains not merged into the crystals, equivalently, not suffering serious interactions by neighboring chains. In the comb-like polymers, the mobile chains (branches) suffer additional constraints due to their 'grafting' onto the backbone of the comb, this being reflected on the retardation of α as compared to the linear OEGMAs, the effect being more pronounced for the short chains. Finally, the OEGMAs demonstrate an additional segmental-like relaxation (α') which exhibits the characteristics of the normal-mode process, namely screening the fluctuation of the chain end-to-end vector. The latter process is not recorded in the POEGMAs, most probably due to the constraints imposed by the one-side 'grafting' of the branches.

Overall, the deeper scope of the design of these materials is achieved, as the expected information on the possibility of tuning crystallization and polymers chain diffusion was successfully extracted by the direct and indirect dielectric techniques. The latter is quite interesting, also from the methodological point of view, and proves once again the dielectric techniques quite power tools with respect to the structure–property relationship investigations.

Conflicts of interest

There are no conflicts to declare.

Acknowledgements

References

1 F. Hua, X. Jiang, D. Li and B. Zhao, *J. Polym. Sci., Part A: Polym. Chem.*, 2006, **44**, 2454–2467.
2 J. F. Lutz, *J. Polym. Sci., Part A: Polym. Chem.*, 2008, **46**, 3459–3470.
3 A. Miasnikova and A. Laschewsky, *J. Polym. Sci., Part A: Polym. Chem.*, 2012, **50**, 3313–3323.
4 R. C. Advincula, W. J. Brittain, K. C. Caster and J. Rühe, *Polymer Brushes*, Wiley-VCH, Weinheim, 2004.
5 H. Shi, Y. Zhao, X. Dong, Y. Zhou and D. Wang, *Chem. Soc. Rev.*, 2013, **42**, 2075–2099.
6 S. Kripotou, Ch Psylla, K. Kyriakos, K. N. Raftopoulos, J. Zhao, G. Zhang, S. Pispas, C. M. Papadakis and A. Kyritsis, *Macromolecules*, 2016, **49**, 5963–5977.
7 I. Yildririm, T. Bus, M. Sahn, T. Yildirim, D. Kalden, S. Hoeppener, A. Traeger, M. Mesterhausen, C. Weber and U. S. Schubert, *Polym. Chem.*, 2016, **7**, 6064–6074.
8 E. Barnard, R. Pfukwa, J. Maiz, A. J. Müller and B. Klumperman, *Macromolecules*, 2020, **53**, 1585–1595.
9 Z. Hu, T. Cai and C. Chi, *Soft Matter*, 2010, **6**, 2115–2123.
10 H. Lomas, I. Canton, S. MacNeil, J. Du, S. P. Armes, A. J. Ryan, A. L. Lewis and G. Battaglia, *Adv. Mater.*, 2007, **19**, 4238–4243.
11 E. S. Gil and S. M. Hudson, *Prog. Polym. Sci.*, 2004, **29**, 1173–1222.
12 Z. An, Q. Shi, W. Tang, C. K. Tsung, C. J. Hawker and G. D. Stucky, *J. Am. Chem. Soc.*, 2007, **129**, 14493–14499.
13 A. Kyritsis, A. Laschewsky and C. M. Papadakis, *Self-assembling of thermo-responsive block copolymers: structural, thermal and dielectric investigations, in Thermodynamics and biophysics of biomedical nanosystems. Series in bioengineering*, ed. C. Demetzos and A. Pippa, Springer, Singapore, 2019, ch. 12, p. 397.
14 H. Sun, D. M. Yu, S. Shi, Q. Yuan, S. Fujinami, X. Sun, D. Wang and T. P. Russell, *Macromolecules*, 2019, **52**, 592–600.
15 K. Inomata, E. Nakanishi, Y. Sakane, M. Koike and T. Nose, *J. Polym. Sci., Part B: Polym. Phys.*, 2005, **43**, 79–86.
16 D. Neugebauer, M. Theis, T. Pakula, G. Wegner and K. Matyjaszewski, *Macromolecules*, 2006, **39**, 584–593.
17 C. Nikovia, L. Theodoridis, S. Alexandris, P. Bilalis, N. Hadjichristidis, G. Floudas and M. Pitsikalis, *Macromolecules*, 2018, **51**, 8940–8955.
18 H. Xu, Y. Gao, J. Li, H. Wang and H. Shi, *Polymer*, 2018, **153**, 362–368.
19 P. C. Ashman and C. Booth, *Polymer*, 1975, **16**, 889–896.

20 A. J. Müller, V. Balsamo and M. L. Arnal, *Adv. Polym. Sci.*, 2005, **190**, 1–63.
21 Y. Suzuki, H. Duran, M. Steinhart, H. J. Butt and G. Floudas, *Soft Matter*, 2013, **9**, 2621–2628.
22 L. Sangroniz, D. Cavallo and A. J. Müller, *Macromolecules*, 2020, **53**, 4581–4604.
23 A. T. Lorenzo, M. Arnal, J. J. Sanchez and A. J. Müller, *J. Polym. Sci., Part B: Polym. Phys.*, 2006, **44**, 1738–1750.
24 M. J. Muthukumar, *Chem. Phys.*, 2016, **145**, 031105.
25 M. Muthukumar, *Prog. Polym. Sci.*, 2020, **100**, 10184.
26 X. Liu, Y. Wang, Z. Wang, D. Cavallo, A. J. Müller, P. Zhu, Y. Zhao, X. Dong and D. Wang, *Polymer*, 2020, **188**, 122117.
27 L. Sangroniz, A. Sangroniz, L. Meabe, A. Basterretxea, H. Sardon, D. Cavallo and A. J. Müller, *Macromolecules*, 2020, **53**, 4878–4881.
28 A. Czaderna-Lekka, K. Piechocki, M. Kozanecki and L. Okrasa, *J. Phys. Chem. Solids*, 2020, **140**, 109359.
29 M. Kozanecki, M. Pastorczak, L. Okrasa, J. Ulanski, J. A. Yoon, T. Kowalewski, K. Matyjaszewski and K. Koyonov, *Colloid Polym. Sci.*, 2015, **293**, 1357–1367.
30 F. Kremer and F. Schönhals, *Broadband dielectric spectroscopy*, Springer-Verlag, Berlin, 2002.
31 D. Fragiadakis, P. Pissis and L. Bokobza, *Polymer*, 2005, **46**, 6001–6008.
32 M. Füllbrandt, P. J. Purohit and A. Schönhals, *Macromolecules*, 2013, **46**, 4626–4632.
33 A. Alegria and J. Colmenero, *Soft Matter*, 2016, **12**, 7709–7725.
34 E. Christodoulou, P. A. Klonos, K. Tsachouridis, A. Zamboulis, A. Kyritsis and D. N. Bikiaris, *Soft Matter*, 2020, **16**, 8187–8201.
35 A. Karatza, P. Klonos, S. Pispas and A. Kyritsis, *Polymer*, 2019, **181**, 121794.
36 Y. Wang, C. B. Liu, L. Y. Fan, Y. Sheng, J. Mao, G. T. Chao, J. Li, M. J. Tu and Z. Y. Qian, *Polym. Bull.*, 2005, **53**, 147–154.
37 P. S. Gill, S. R. Sauerbrunn and M. Reading, *J. Therm. Anal. Calorim.*, 1993, **40**, 931–939.
38 Y. Suzuki, H. Duran, W. Akram, M. Steinhart, G. Floudas and H. J. Butt, *Soft Matter*, 2013, **9**, 9189–9198.
39 S. Havriliak and S. Negami, *Polymer*, 1967, **8**, 161–210.
40 J. Van Turnhout, *Front. Chem.*, 2016, **4**, 22.
41 N. M. Alves, J. F. Mano, E. Balaquer, J. M. Meseguer Dueñas and J. L. Gómez Ribelles, *Polymer*, 2002, **43**, 4111–4122.
42 S. Montserrat, J. L. Gómez Ribelles and J. M. Meseguer, *Polymer*, 1998, **39**, 3801–3807.
43 J. M. G. Cowie and I. J. McEwen, *Polymer*, 1973, **14**, 423–426.
44 J. Dobbertin, A. Hensel and C. Schick, *J. Therm. Anal. Calorim.*, 1996, **47**, 1027–1040.
45 U. Gaur and B. Wunderlich, *J. Phys. Chem. Ref. Data*, 1981, **10**, 1001–1049.
46 R. Androsch, C. Schick and A. M. Rhoades, *Macromolecules*, 2015, **48**, 8082–8089.
47 A. Toda, R. Androsch and C. Schick, *Polymer*, 2016, **91**, 239–263.
48 P. A. Klonos, S. N. Tegopoulos, C. S. Koutsiara, E. Kontou, P. Pissis and A. Kyritsis, *Soft Matter*, 2019, **18**, 1813–1824.

49 R. M. Michell, A. Mugica, M. Zubitur and A. J. Müller, *Adv. Polym. Sci.*, 2017, **276**, 215–256.

50 Z. Terzopoulou, P. A. Klonos, A. Kyritsis, A. Tziolas, A. Avgeropoulos, G. Z. Papageorgiou and D. N. Bikiaris, *Polymer*, 2019, **166**, 1–12.

51 R. Boehmer, K. Ngai, C. A. Angell and D. J. Plazek, *J. Chem. Phys.*, 1993, **99**, 4201–4209.

52 P. Klonos, P. Pissis, V. M. Gun'ko, A. Kyritsis, N. V. Guzenko, E. M. Pakhlov, V. I. Zarko, W. Janusz, J. Skubiszewska-Zięba and R. Leboda, *Colloids Surf., A*, 2010, **360**, 220–231.

53 P. Klonos, S. Kaprinis, V. I. Zarko, V. Peoglos, E. M. Pakhlov, P. Pissis and V. M. Gun'ko, *J. Appl. Polym. Sci.*, 2013, **128**, 1601–1615.

54 S. Kripotou, P. Pissis, P. Sysel, V. Sindelar and V. A. Bershtein, *Polymer*, 2006, **47**, 357–366.

55 D. R. Figueroa, J. J. Fontanella, M. C. Wintersgill, J. P. Calame and C. G. Andeen, *Solid State Ionics*, 1988, **28–30**, 1023–1028.

56 I. M. Kalogeras, M. Roussos, I. Christakis, A. Spanoudaki, D. Pietkiewicz, W. Brostow and A. Vassilikou-Dova, *J. Non-Cryst. Solids*, 2005, **351**, 2728–2734.

57 M. Miyara, I. Takashima, K. Sasaki, R. Kita, N. Shinyashiki and S. Yagihara, *Polym. J.*, 2017, **49**, 1–8.

58 M. Dionísio and M. T. Viciosa, *Polymer*, 2018, **148**, 339–350.

59 M. Carsi, M. J. Sanchis, R. Diaz-Calleja, E. Riande and M. J. D. Nugent, *Macromolecules*, 2012, **45**, 3571–3580.

60 G. P. Johari and M. Goldstein, *J. Chem. Phys.*, 1970, **53**, 2372–2388.

61 G. Tammann and W. Hesse, *Z. Anorg. Allg. Chem.*, 1926, **156**, 245–257.

62 D. Fragiadakis and P. Pissis, *J. Non-Cryst. Solids*, 2007, **47–51**, 4344–4352.

63 J. Ren, O. Urakawa and K. Adachi, *Polymer*, 2002, **44**, 847–855.

64 A. Schönhals, H. Goering and C. Schick, *J. Non-Cryst. Solids*, 2002, **305**, 140–149.

65 A. Kyritsis, P. Pissis, S. M. Mai and C. Booth, *Macromolecules*, 2000, **33**, 4581–4595.

66 W. W. Graessley in *Synthesis and degradation rheology and extrusion. Advances in Polymer Science*, ed. H. J. Cantow, *et al.*, Springer, Berlin Heidelberg, 1982, vol. 47, pp. 67–117.

67 R. Richert, A. Agapov and A. P. Sokolov, *J. Chem. Phys.*, 2011, **134**, 104508.